UNMANNED SYSTEMS

http://www.worldscientific.com/worldscinet/us

Design and Implementation of a Thrust-Vectored Unmanned Tail-Sitter with Reconfigurable Wings

Kevin Z. Y. Ang*,§, Jin Q. Cui†,¶, Tao Pang‡,‖, Kun Li*,**, Kangli Wang*,††,
Yijie Ke*,‡‡, Ben M. Chen*,§§

*Unmanned System Research Group,
The National University of Singapore, Singapore 117583

†NUS Graduate School for Integrative Sciences and Engineering,
The National University of Singapore, Singapore 117456

‡Temasek Laboratories,
The National University of Singapore, Singapore 117411

In this paper, we present the development of a reconfigurable hybrid unmanned aerial vehicle (UAV): U-Lion [Ang et al., 11th IEEE Int. Conf. Control Automation (ICCA), pp. 750–755]. U-Lion is a small-scale UAV that is capable of vertical takeoff and landing (VTOL) and fixed-wing Cruise modes through its unique mechanical design. Mainly built with carbon fiber and expanded polyolefin (EPO) foam, U-Lion is equipped with an array of avionic components which enable stable control of the UAV both in VTOL and Cruise modes. It was employed by the National University of Singapore (NUS) Unmanned System Research Group to participate in the 2013 UAV Grand Prix (UAVGP) competition held in Beijing, China. Its design adopts a reconfigurable wing and a tail-sitter structure, which combines the advantages of a fixed-wing plane and a rotor helicopter effectively. U-Lion could transit from vertical takeoff to a hovering stage before flying in Cruise mode to realize efficient long duration flight. The propulsion of U-Lion comes from a self-fabricated contra-rotating motor fixed on a gimbal mechanism which can change the direction of the motor for the required thrust. This thrust-vectored propulsion system primarily provides control in the VTOL mode but also enhances flight capabilities in Cruise mode. The maximum thrust provided by the motor can be as high as 40 N and it provides six degree of motion controls in VTOL mode. U-Lion has a few special internal designs to empower its capabilities: (1) Reconfigurable wings allow the U-Lion to adapt to different flying modes. (2) Adaptive center of gravity (CG) by adjusting the battery position to fulfill the different requirements of CG for VTOL mode and Cruise mode. (3) Unique contra-rotating thrust-vectored propulsion system. The detailed design and implementation procedure have been presented in this paper along with our computational fluid dynamics (CFD) simulation results, real flight tests and competition performance.

Keywords: Thrust-vectored; tail-sitter; reconfigurable wing; unconventional UAV.

1. Introduction

Development of unconventional unmanned aerial vehicles (UAVs) have made major progress due to the huge improvements in research areas such as UAV flight control

theories, micro-electro-mechanical systems (MEMS), electronic devices and material science. Unconventional UAVs have great potential applications in military and civilian operations, especially where there are severe constraints in their operating environment. In tasks such as outdoor surveillance, the ability to perform long endurance or long distance missions usually requires the UAV to perform cruising flight. An efficient cruising flight is usually achieved with UAVs having airfoils that have good lift-to-drag ratios. However, there are cases where there is insufficient take-off space available for standard airplane-type UAVs to be

launched and recovered. On the other hand, the capability of vertical takeoff and landing (VTOL) and hovering is beneficial to most surveillance missions as it allows for a close up static surveillance view of the intended target instead of circling around the target site as with most fixed-wing UAVs. A hybrid UAV with both cruising flight and VTOL capability will be very useful in such tasks. A few prototypes of hybrid aircrafts fitting these tasks have been designed in the past, such as the tail-sitter airplanes jointly developed by the University of Sydney and the University of Compiegne [2], the hybrid UAV developed by icarusLabs [3] and the tilting-wing quadrotor [4], SUAVI, developed by Hancer and his teammates.

However, these existing designs are usually only optimal in one mode of flight and largely sacrifice the performance of the other mode. For example, the main structural design of SUAVI ensures its stable flight in the VTOL mode. However, its airfoil structure designed for the Cruise mode is just four small pieces of airfoils attached to the tilting wings. The Cruise mode is inefficient as compared to normal airplanes. It is also very sensitive to wind disturbances during its hovering. These kinds of shortcomings are mainly due to the designed platform's inability to reconfigure its shape or wingspan area. The tail-sitter UAV on the other hand is optimal in its Cruise flight as it encompasses large airfoils while it sacrifices VTOL performance as these airfoils usually create disturbances in VTOL control when wind gusts are present [5]. Tail-sitter UAVs also require a diving maneuver for the UAV to transit from VTOL mode to Cruise mode [6]. If both modes of flight need to be optimized, a reconfigurable aircraft structure design might be a solution. Moreover, the control problem of smooth transition between the VTOL and Cruise modes of a hybrid aircraft is still at its initial stage.

The NUS Unmanned System Research Group has started researching into hybrid aircraft in the recent years and the ideology was to create a hybrid UAV that could achieve optimal flight performances in both VTOL and Cruise mode. In this paper, we propose a systematic design and development methodology that enables us to rapidly develop U-Lion. U-Lion is the preliminary prototype developed by the group which not only has two modes of flight, but is also capable of restructuring the platform shape by folding or expanding its wings. This special design aims to achieve stable and efficient flight in both VTOL and Cruise modes. Through many alterations, U-Lion is an improved version of the reconfigurable horizontal/vertical transition UAV which performs much better in both modes of flight and has a bi-directional smooth transition.

The NUS UAV team took part in the 2nd AVIC Cup International UAV Innovation Grand Prix (UAVGP) which is a large-scale biennial aviation event authorized by the Ministry of Science and Technology, and co-organized by the Aviation Industry Corporation of China and Chinese Society of Aeronautics and Astronautics, hosted by AVIC Culture Co. Ltd. As an aviation mega festival, UAVGP provides an opportunity to show innovative ideas and new technological works, as well as act as a platform of international communication for individuals and groups all over the world. The UAVGP comprises several different competition categories such as the Athletic Grand Prix, the Creativity Grand Prix and the Air Show competition. U-Lion was registered into the Creativity Grand Prix along with 76 other teams. In the Creativity Grand Prix, competitors had to design a new type of aircraft that has unique characteristics and prove that it was capable of stable flight and has potential applications. The NUS team garnered the New Innovation Star Award for U-Lion's unique features.

Since the development of a UAV dwells into many different fields of work, we will cover each portion that is vital to U-Lion's construction. The remainder of this paper is organized as follows: Our design methodology and philosophy is presented in Sec. 2. In Secs. 3 and 4, we describe some of our previous prototypes and show how we iteratively improved our design to the current U-Lion. The detailed design of mechanical structure, electronic components, fluid dynamics and control are then shown in Sec. 5. Finally, we draw some concluding results in Sec. 6.

2. Design Methodology

Our design methodology with reference from Cai *et al.* [9] was an iterative way of four steps shown in Fig. 1. The first step of our design was overall layout design, which includes the brainstorming process, aircraft configuration establishment and weight estimation. The second step includes: (I) Wing design, in which we designed the wing based on parameters that can satisfy our requirement for the lift force. (II) Propulsion design, in which we designed the
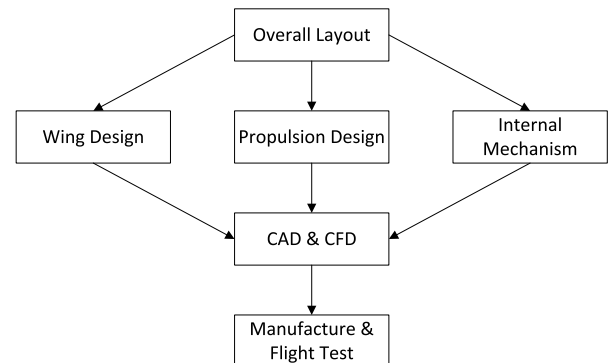

Fig. 1.   Design methodology.

propulsion system comprising rotors and gimbals. (III) Internal mechanisms design, several mechanisms were designed to realize reconfigurable wings, adaptive CG and canard wings. The third step was generating the computer-aided design (CAD) and computational fluid dynamics (CFD) analysis. This step allowed us to realize and validate our design virtually. We designed all the components and parts for our UAV in detail, and exported the geometry to the CFD software to validate their aerodynamic performance. We may have several iterations in this step until all of the design specifications are satisfied. The last step is implementation and flight test. Carbon fiber and EPO foam were used as the materials for U-Lion because of their low weight and good structural characteristics. Flight tests were then conducted for our U-Lion including VTOL tests and fixed-wing tests until the platform's flight performance met our expectation.

The design of this unconventional UAV was motivated by the requirements of unconventional UAVs with the capacities of VTOL, hovering and long-range, high-speed flight. The requirement of VTOL led to the incorporation of a rotary propulsion feature in our design. Although the flapping-wing mechanism is also a popular concept in VTOL, difficulties involve flexible structural dynamics, bio-inspired mechanisms and advanced flight control technology, and they cannot be easily overcome in the near future [7]. For the rotary propulsion approach, single-rotor configuration will induce a rotating torque to the main body which is often compensated by a tail rotor and a constant control surface deflection, so we adopt contra-rotating propulsion which eliminates this rotating torque problem. Co-axial rotary propulsion is another propulsion approach, which makes use of two contra-rotating motors to counter the torque, providing a compact solution to balancing the torque in the yaw direction. For the roll and pitch dynamics, traditional co-axial rotors require swashplates to change the pitch angle of the rotors. The complexity of the swashplates makes it difficult for such mechanisms to be applied to small-scale UAVs. We come up with a fixed-pitch co-axial rotor design with vector thrust which is realized by a gimbal mechanism activated by two electric servos, whereby the pitch and roll channels are mechanically decoupled. The yawing motion is achieved by the difference of the upper and lower rotor rotational rates.

There are also some other hybrid aircrafts adopting multi-rotor system as their propulsion methods. The Tactical Utility TU-150 from Rheinmetall Airborne Systems [8], with two propeller blades mounted on its wing tips, is capable of hovering and cruising at 120 knots for up to 8 h. Some research groups take the quad-rotor design as the VTOL scheme, distributing four rotors on the wing and fuselage. Certain rotors are able to tilt forward to provide propulsion for fixed-wing flight. However, limited by thrust provided and weight budget, the multi-rotor option, subjected to low efficiency and large weight, is not an ideal choice. With these considerations, the vector thrust with a gimbal mechanism outperforms other approaches with regards to weight, design complexity and energy efficiency.

The mission of long-range flight and high cruising speed brings about several problems. Wing shape, configuration and its layout are main factors that affect the efficiency, which are relative to the endurance, maximum velocity, as well as the maneuverability.

The wing shape is typically defined by aspect ratio. The aspect ratio is a measurement of how long and slender the wing appears when seen from above. Generally, wings are categorized into low, moderate and high aspect ratio according to different length-to-breadth ratio. Airplanes with low aspect ratio wings are more structurally efficient and have higher instantaneous roll rate. Low aspect ratio planes allow for high and ultra high speed, and more aggressive maneuverability. The moderate aspect ratio wings are made for most of the general purpose aircrafts with requirements on moderate velocity and endurance. For the high aspect ratio wings, with a long and slender appearance, they are applied to the aircrafts capable of long range and extremely stable Cruise flight due to aerodynamical efficiency of the wings and less induced drag. For this unconventional UAV, the moderate aspect ratio (between 2 and 7) are selected due to the tradeoff between high speed and long endurance.

Wing sweep angle is one of the main factors that affect the aerodynamic characteristics and efficiency of wings. The straight wings are the most structurally efficient ones that are adopted by the majority of low-speed aircraft designs. Some wings sweep forward from the root to the tip to avoid tip stall problems and reduce tip losses, while forward swept wings are subject to aeroelastic flutter. The example of forward swept wings can be found on the design of Su-45 Berkut. However, swept wings aircraft are often developed with the wings sweeping rearwards from the root to the tip. Positive wingsweep is usually used to delay the onset of Mach effects at higher Mach speeds. In supersonic flight, if the leading edge is still subsonic, the aircraft will be able to achieve higher maneuverability as you do not have the full neutral point shift.

Although our aircraft does not reach supersonic flight, we designed variable sweep wings which give us configurable wing positions such that the wings could be adjusted at different occasions to suit different operational needs such as landing and Cruise flight. A four-bar mechanism was developed to meet the requirement of wing repositioning in our design and will be describe in Sec. 5.4.

In the following, we will describe in detail how we performed our design iteration before arriving at the final prototype which is U-Lion in Sec. 5.

3.   Preliminary Design

Wing design is the most crucial part for an aircraft design, as the lift created by the wings needs to exceed the gravitational force by around 50% to 100% to provide enough control margin. To describe the performance of wings, several parameters are generally used including the lift coefficient C_L, drag coefficient C_D and wing loading. These characteristics are affected by aircraft forward velocity, angle of attack (AOA) and wing airfoil shape [13]. The following formulae represent the lift coefficient and drag coefficient,

$$C_L = \frac{2L}{\rho v^2 A}, \tag{1}$$

$$C_D = \frac{2F_d}{\rho v^2 A}, \tag{2}$$

where L is the lift force, F_d is the drag force, ρ is the mass density of the fluid, v is the speed of the object relative to the fluid, which is actually flight speed, and A is the reference area, which is the wing area.

In our design, we make use of the lift and drag coefficient to estimate the expected operational lift we could generate at differing AOA [12]. This allows us to know how the aircraft will perform while cruising and to know the minimum velocity it must achieve to generate sufficient lift for the whole aircraft.

3.1.   *Wing design*

Several airfoil candidates from National Advisory Committee for Aeronautics (NACA) are analyzed with the toolkit "XFOIL" [10] by MIT, with regard to the lift coefficient, drag coefficient as well as the pressure distribution among the surface of the airfoil. U-Lion was envisaged to fly at relatively low speeds of around 5–15 m/s, resulting in a low Mach number and Reynolds number. Also, the AOA of a fixed-wing aircraft generally varies between 2° and 10°. Thus, the airfoil analysis is under inviscid air situation. Airfoil selection targets on large lift-coefficient, low drag coefficient at small attack angle and flying speed. Several parameters involved in the Xfoil simulation are Mach number and Reynolds number, which are calculated as follows:

$$M = \frac{V}{V_{\text{sound}}} = \frac{10}{340} = 0.029, \tag{3}$$

$$\text{Re} = \frac{Vc}{v} = \frac{10 \times 0.4}{1.460 \times 10^{-5}} = 274{,}000, \tag{4}$$

where M is the Mach number, Re is the Reynolds number, V is the forward velocity of the aircraft, V_{sound} is the velocity of sound at normal condition, c is the average chord line of the
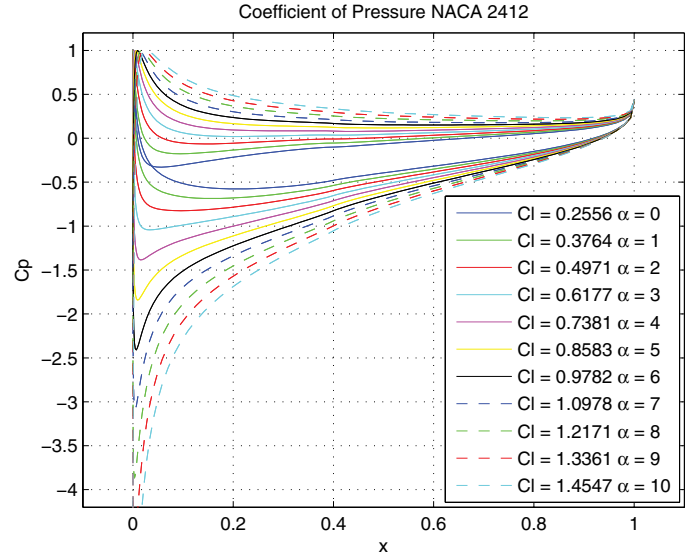

Fig. 2.   Lift coefficient and pressure coefficient C_p distribution of NACA airfoil 2412.

wing, which is 0.4 m and v is the kinematics viscosity of the atmosphere at sea level, which is $1.460 \times 10^{-5}\,\text{m}^2/\text{s}$.

Figure 2 shows the influence of wing AOA to the lift coefficient of NACA airfoil 2412. The relationships of lift coefficient, pressure distribution and AOA are presented in the figure. Lift coefficient increases with AOA in an allowable range from 0° to 10°. The pressure coefficient C_p is plotted corresponding to different locations of the airfoil. The pressure coefficient is calculated as:

$$C_p = \frac{p - p_\infty}{\frac{1}{2}\rho_\infty V_\infty}, \tag{5}$$

where p is the pressure at the point, p_∞ is the pressure in the freestream, ρ_∞ is the freestream fluid density and V_∞ is the velocity of the freestream fluid. From the pressure coefficient of the points of the airfoil surface, the lift coefficient can be integrated with the following formula,

$$C_l = \int_{\text{LE}}^{\text{TE}} (C_{pl}(x) - C_{pu}(x))d\frac{x}{c}, \tag{6}$$

where LE is the leading edge, TE is the trailing edge, c is the chord length, C_{pl} and C_{pu} are the pressure coefficients of upper and lower surface of the airfoil. With the pressure coefficient, the lift coefficients are calculated by numerical integration and displayed in the second column at the right side of Fig. 2. It is illustrated in the legend of the figure that in the operating range of wing AOA, lift coefficient increases with the increment of the AOA.

Figure 3 shows the aerodynamic characteristics of NACA asymmetrical airfoils with different maximum camber positions, which are NACA 2412, 2512, 2612 and 2712.
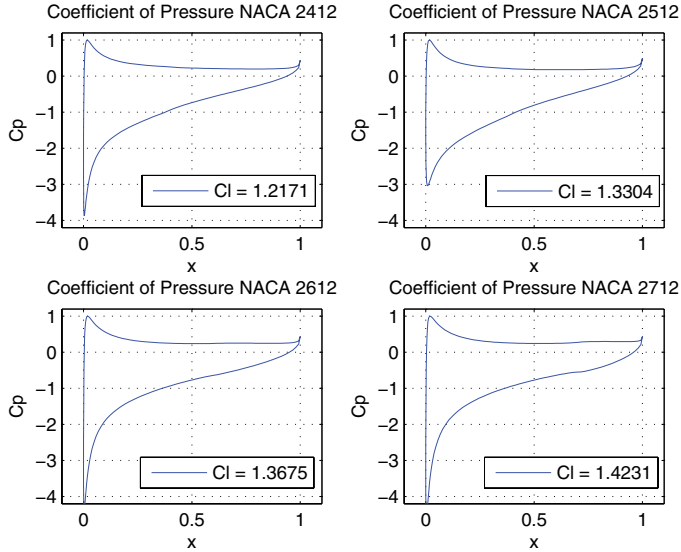
Fig. 3. Aerodynamic features of airfoils with different maximum camber positions.

Here, Mach number and Reynolds number are kept the same and AOA is fixed at $8°$. From the figure, it is known that both the lift coefficient and the drag coefficient increase with the maximum camber position shifting from the leading edge to the trailing edge. Figure 4 shows the change of airfoil aerodynamic features with different maximum camber values, which are NACA airfoil 3412, 4412, 5412 and 6412, respectively. We can see from the figure that high camber value airfoils result in higher lift, while they also bring high drag force and require increasing stiffness. The relationship of airfoil characteristics and their thickness is
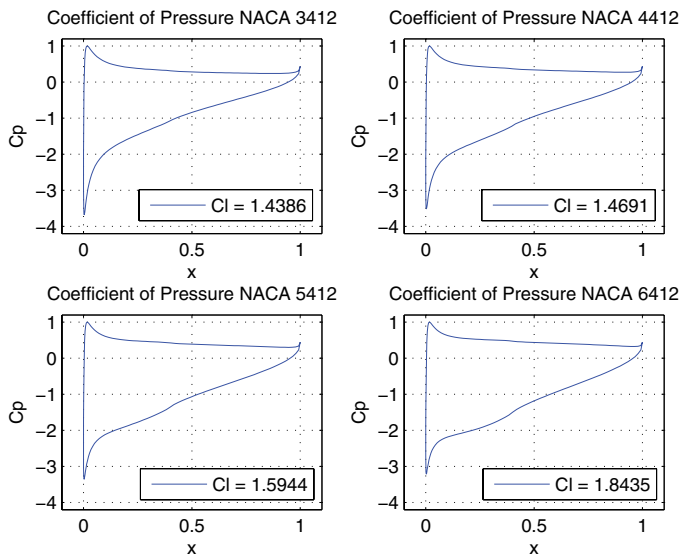
Fig. 4. Aerodynamic features of airfoils with different maximum camber values.
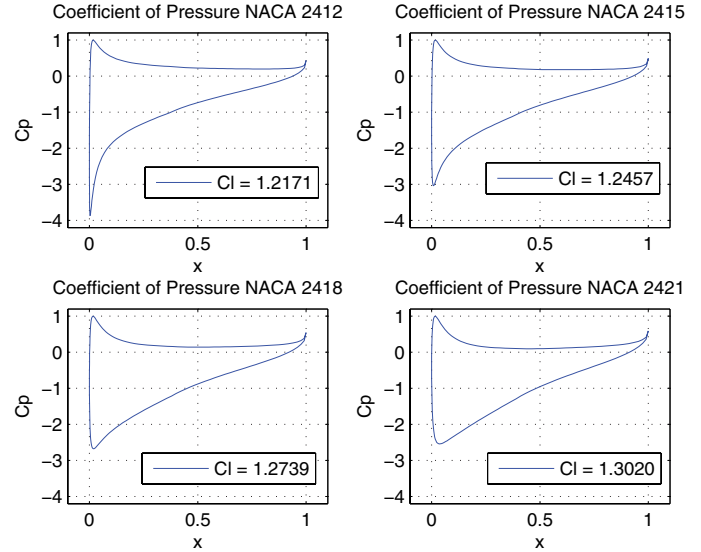
illustrated in Fig. 5. A series of NACA airfoils 2412, 2415, 2418 and 2421 are selected to investigate the relevance. It is obvious in Fig. 5 that thicker airfoils create higher lift and drag, due to the large difference between the flow distances at the upper surface and lower surface.

Selection of wings are based on several factors, including the aerodynamic and mechanical considerations. From the specifications described in Sec. 2, lift created by wings, drag force, forward velocity and AOA are the main factors that need to be considered:

(1) Lift coefficient. According to the design specification, at the default AOA of $8°$ and velocity of $10\,\text{m/s}$, the wings are to generate lift force to elevate its own weight, at a maximum of 2 kg. The required value of lift coefficient can be obtained by the desired force, air density, forward velocity and wing area (see Eq. (1)).
(2) Drag coefficient. When the aircraft was shifted to fixed-wing mode, the forward propulsion is provided by the vectored thrust, which is large enough to lift the whole take-off weight at VTOL mode. Thus, the drag coefficient is not a main concern due to a large forward thrust.
(3) Assembly concern. The aircraft is designed to be a variable sweep wing, and wings are able to be fully closed at VTOL mode to reduce the whole rotating torque of yawing motion. This design requires that the wings are thin and smooth enough to be easily retracted into the fuselage. Thus, the thickness is a main consideration.

According to the discussion above, the NACA airfoil 2712, which has a maximum camber of 2% located 70% from the leading edge with a maximum thickness of 12% of the chord, is selected. From Fig. 3, at AOA of $8°$, the lift coefficient reaches 1.4231 at velocity of $10\,\text{m/s}$.

Fig. 5. Aerodynamic features of airfoils with different thickness.

3.1.1. *Wing design in virtual environment*

Wing design in virtual environment is essential to provide a broad overview of wing functionalities and size. A 3D mechanical design software named SolidWorks, developed for efficient and quicker design of mechanical products and components, facilitates the design tasks for the platform.

With the wing airfoil NACA 2712 selected, the wing layout is to be designed to meet the specifications and functionalities. On one hand, the wing area needs to be large enough to create lift force to elevate the platform. On the other hand, the wings are able to be retracted into the fuselage and fully covered as a unitary VTOL aircraft. With these purposes, the design procedures with the aid of SolidWorks are listed below:

(1) The airfoil is imported and scaled to the actual UAV size, with a chord length of 500 mm (see Fig. 6(a)).
(2) To create the wing shape with a swept back angle, a triangular structure is first lofted with two sketches, shown in Fig. 6(b). A part of the wing at the trailing edge is removed to realize variable swept back angle, as shown in Fig. 6(c).
(3) Another part of the wing is removed to avoid interference between wing and fuselage. A joint connecting to

(a) (b)

(c) (d)

(e) (f)
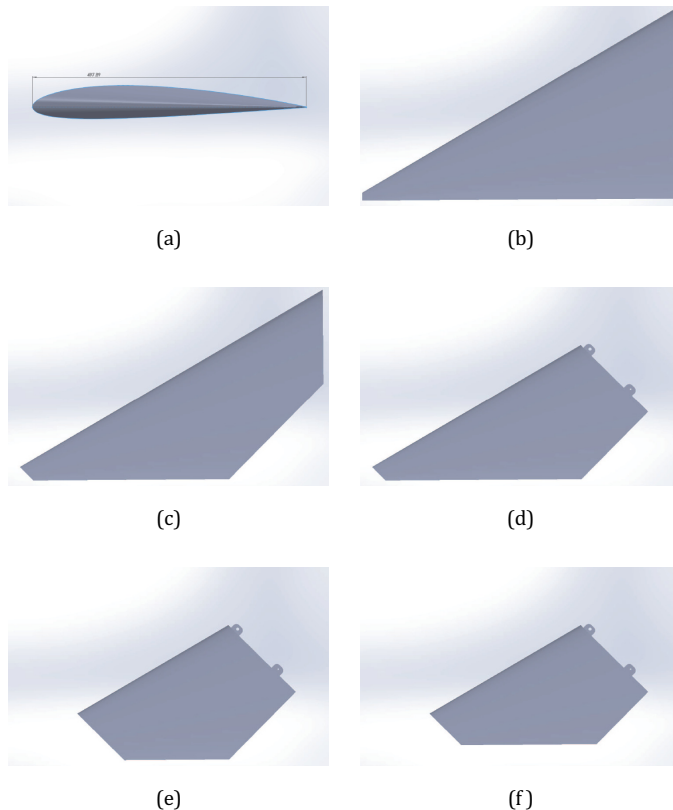
Fig. 6. Wing design procedures with SolidWorks.

the fuselage and a pivot connecting to 4-bar mechanism are created at the cutting facet, as displayed in Fig. 6(d).
(4) The whole wing structure is shortened from the tail (Fig. 6(e)) to ensure that the wings are inline with the empennage at the VTOL mode.
(5) A bar is separated from the main wing at the trailing edge, serving as the control surface, which is hinged to the main wing, as illustrated in the last step.

Area of the wing measured in the virtual environment is 0.12 m², and the lift force created by one single wing is given by,

$$L = \frac{1}{2}C_L\rho v^2 A_p = 10.13\,\text{N},$$

where A_p is the projected area at a certain AOA. The result indicates that the wings are able to provide a thrust of 20 N, equivalent to a 2 kg platform.

3.2. *Fuselage design*

In the above section, the theoretical calculation show that the wings are capable of lifting a 2 kg platform at the flight speed of 10 m/s and AOA at 8°. However, this occasion is an ideal case, with respect that the take-off speed and the transformation speed are less than 10 m/s and AOA cannot be maintained at 8° accurately in real flight due to the disturbance and pilot maneuver. Consequently, the margin for lift generation is indispensable for this hybrid UAV design, which leads to the development of a fuselage with multiple functionalities as follows:

(1) The fuselage is also capable of providing lift at Cruise flight mode, i.e., a fuselage with certain asymmetric airfoil.
(2) There is a cavity design in the fuselage to include all the components, e.g., the battery, the servos, the 4-bar mechanism and gyros, as well as a lid for easily accessing the inner components. An additional cavity design to place the wings at VTOL mode needs to be reserved.
(3) Other features to be mounted on the fuselage, e.g., the canard, the vectored-thrust and the empennage.

The NACA airfoil 6721 is selected for the fuselage design due to its high lift coefficient and thickness, which provides enough space for placing the components and wings. Aerodynamic characteristics can be viewed in Fig. 7 at the same condition of the wings. Procedures of designing the fuselage is described as follows.

(1) NACA airfoil 6721 with a chord length of 900 mm is loaded with the part at trailing edge of 830 mm removed to mount the empennage.
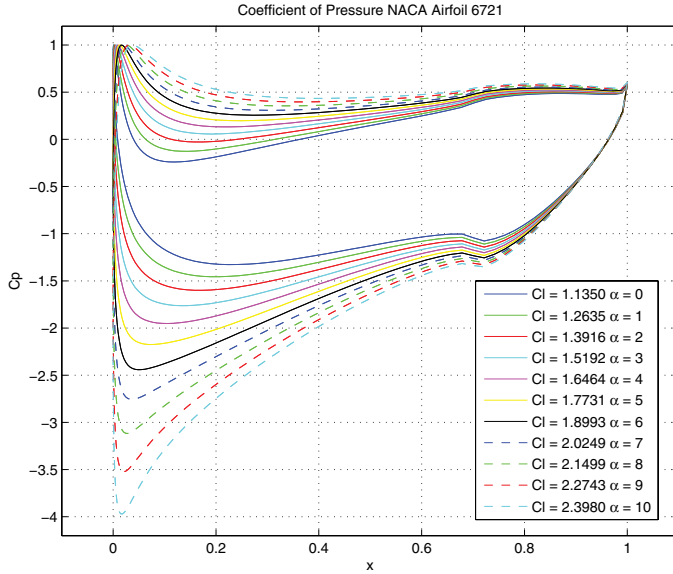
Fig. 7. Lift coefficient and pressure coefficient C_p distribution of NACA airfoil 6721.

(2) The airfoil is lofted following the guide curves shown in Fig. 8(b). The guide curve is designed to reduce drag force.
(3) An extrusion of NACA 6721 is to enlarge the volume of the fuselage so that more space are created to place the wings and inner components.
(4) A mirror operation in Fig. 8(d) is done to obtain the complete outline.
(5) The nose part is designed to facilitate the mounting of the vectored-thrust (see Fig. 8(e)).

The assembly view is displayed in Fig. 9. Wings are fixed at the position for fixed-wing flight mode.

3.3. *XFLR5 simulation*

Functionalities of the hybrid aircraft are first verified with simulation tools XFLR5. By creating a virtual wind tunnel, some basic features including the lift force, drag force, the stability, rolling and pitching momentum can be roughly estimated. XFLR5 is a software developed by Drela from MIT, focusing on analysis for airfoils, wings and planes operating at low Reynolds numbers. Airfoils for wings and fuselage, which are NACA 2712 and NACA 6721, are simulated and analyzed in the previous sections. In this section, simulations mainly focus on the aerodynamic characteristics of the overall structure developed in SolidWorks.

In Fig. 11, relationships among AOA, lift coefficient C_L, drag coefficient C_D and pitching moment coefficient C_M are investigated based on the simulation software. Here, the
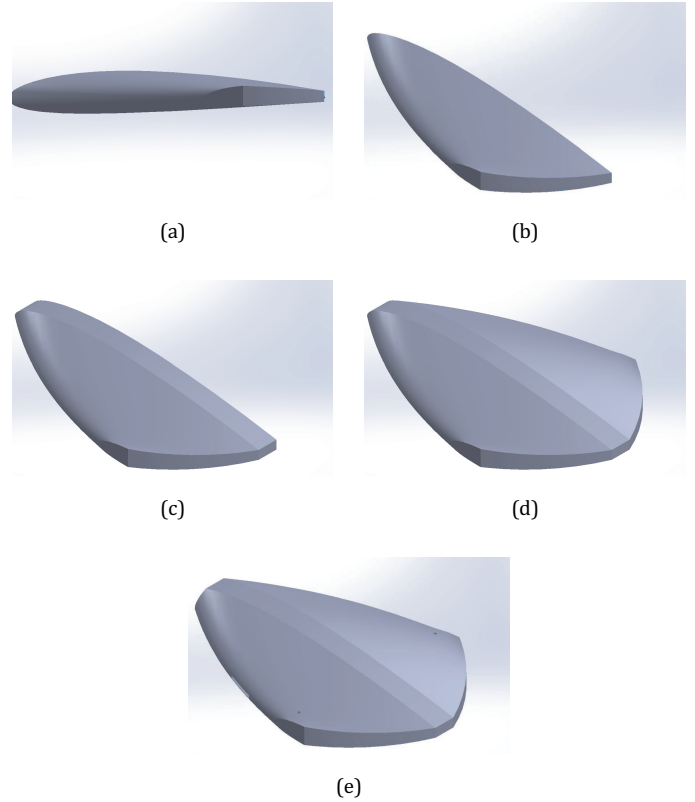

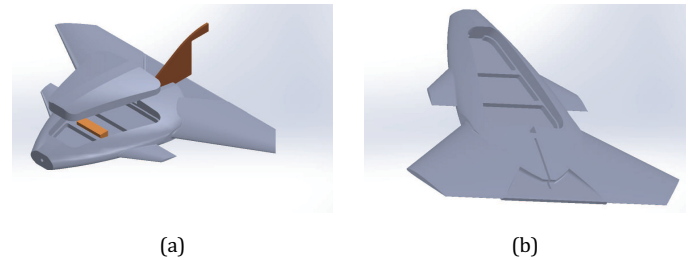Fig. 8. Fuselage design procedures with SolidWorks.

Fig. 9. Assembly effect in SolidWorks.

pitching moment coefficient C_M is defined as,

$$C_M = \frac{M}{qSc}, \tag{7}$$

where M is the pitching moment, q is the dynamic pressure, S is the platform area and c is the chord length of the airfoil. For a flying wing, the pitching moment coefficient is fundamental to the definition of aerodynamic center (AC), which does not vary significantly over the operating range of AOA of the airfoil. Figure 11(a) shows the relation of lift coefficient against AOAα is approximately directly proportional. Figure 11(d) shows the real lift of the aircraft with a whole effective area of $5290\,\mathrm{cm}^2$ at Cruise speed around
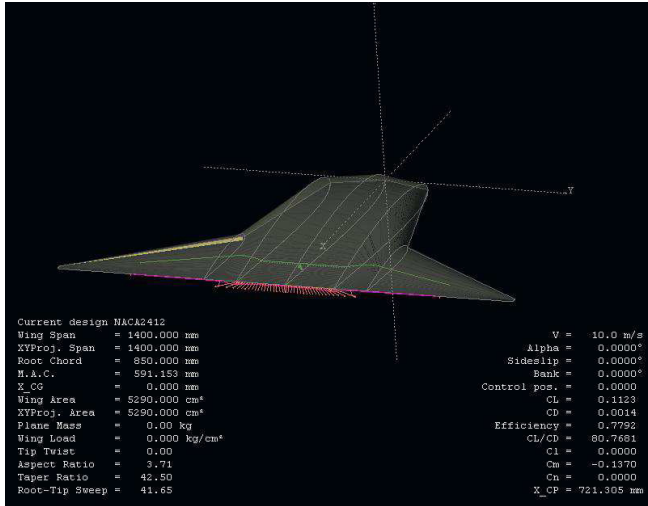
Fig. 10.   XFLR5 simulation of the U-Lion Mark I.

Fig. 12.   Correlation between lift coefficient and pitching moment coefficient.

10 m/s (see Fig. 10) and a lift of 20 N (the platform is assumed to be 2 kg) is achievable at AOA of 10°. The drag coefficient reaches 0.1 at the working range of lift coefficient at 1. As a vectored thrust is mounted in front of the fuselage, the drag force is countered by the thrust. In Fig. 11(c), the relationship of pitching moment coefficient and AOA is given to investigate the aircraft stability at the Cruise flight mode. The relevance can be estimated as an inverse proportion, which is one criteria for a self-stable flying wing. However, at 0 pitching moment ($C_M = 0$), the lift coefficient is negative (see Fig. 12), indicating that at

stable status there is no lift to elevate the aircraft [16]. Thus, the aircraft needs to be controlled with the control surfaces, i.e., aileron, elevator and rudder.

3.4.   *Flight test*

To verify the Cruise flight ability, the whole platform is manufactured by expanded polypropylene (EPP) foam with the wings fixed and rigidly connected to the fuselage at the opening position. Figure 13 shows the platform including the vectored-thrust, control surfaces and all the electronics inside. Nevertheless, the platform was not able to take off due to several possible reasons:

(1) Lift force is not enough to support the whole platform, since the air flow is possibly disturbed by the

Fig. 11.   Aerodynamic analysis of U-Lion Mark I with XFLR5. (a) CL versus AOAα, (b) CL versus CD, (c) CM versus AOAα and (d) lift versus AOAα.

Fig. 13.   U-Lion Mark I.

vectored-thrust, resulting in very low lift coefficient along with the fuselage part.

(2) The weight of the whole assembly is over budget and no more lift is reserved for transformation from VTOL mode to Cruise flight mode.

(3) Drag force is more influential than the simulation results, as a result of coarseness of the EPP foam cut by CNC machine.

(4) Placement of center of gravity (CG) and AC is not reasonable so that the aircraft is not stable after taking off.

Based on these analysis according to its performance in the real flight test, solutions are brought out to improve the hybrid aircraft in the next prototype.

4. U-Lion Mark II

In the prototype Mark II, several modifications are adopted on account of the problems described in the last section. Accordingly, the solutions are as follows:

(1) Low lift force: Higher lift coefficient airfoils are selected compared with NACA 2712 in the first prototype. Wings are lengthened to wingspan 1.6 m compared with 1.2 m in Mark I.

(2) Weight problem: EPP foam with lower density (24 g/l instead of 32 g/l) is adopted. Some internal supporting structures are designed with hollowed parts and aluminum materials are replaced with carbon-fiber sheet.

(3) High air friction: We polish the surface of the raw parts from the CNC machine and attach stickers to create a smooth surface.

(4) Reposition of CG and AC: In the first prototype, the fuselage is too long to locate the aircraft CG in the correct position, which is around 40% from the leading edge of wing for delta shape. Small swept back angle delta shape is adopted in prototype Mark II and the canards are removed to make the aircraft more compact.

4.1. *Wing and fuselage design*

Based on the solutions above, wings with a high lift airfoil are incorporated so that the necessary lift is achievable at relatively small attack angle or lower speed. After searching and comparing a lot of candidates, an airfoil with codename of CH10SM is selected due to its compact shape and high performance. Figure 14 shows the shape of the airfoil CH10SM and its pressure coefficient at cruise speed of 10 m/s and AOA varying from $0°$ to $8°$.

The simulation results are given by XFoil. As AOA equals $8°$, the lift coefficient reaches 2.3541, which is too high for the practical cases. While compared with NACA 2412 used
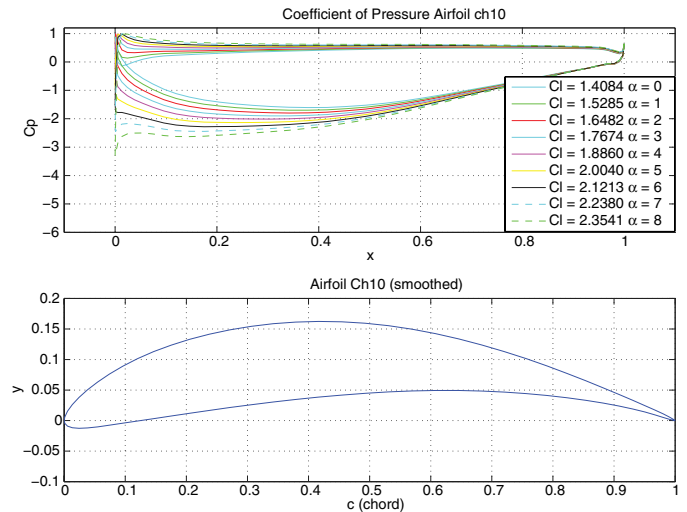

Fig. 14. Lift coefficient and pressure coefficient C_p distribution of airfoil CH10SM.

in prototype Mark I, which is 1.2171 at AOA $= 8°$, the lift coefficient nearly doubles its value in the simulation.

For the fuselage, the airfoil shape was kept the same as Mark I, as the NACA airfoil 6721 is thick enough to include the wings inside the fuselage body and the aerodynamic features also exhibit high performance. Figure 15(a) shows the SolidWorks design of wings and Fig. 15(b) gives the 3D view of the fuselage. In Fig. 16, wings and the fuselage are assembled.
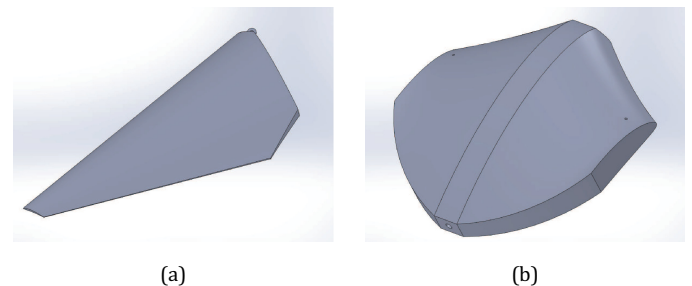

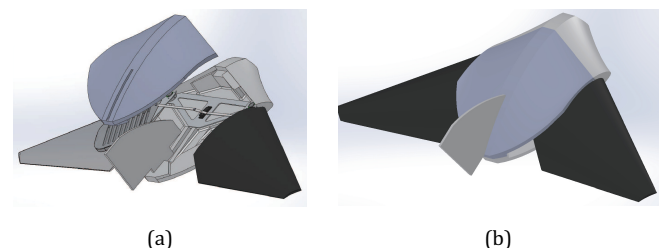Fig. 15. Parts of prototype U-Lion Mark-II.

Fig. 16. Assembly effect in SolidWorks.

4.2.   *XLFR5 simulation*

The model assembled in SolidWorks was exported to XFLR5 for simulation purpose to investigate its aerodynamic properties and stability issues. Figure 17 shows the model in the simulation GUI of XFLR5. The conditions are set as the same case with Mark I, of which the Cruise speed is 10 m/s and the weight is 2.1 kg.

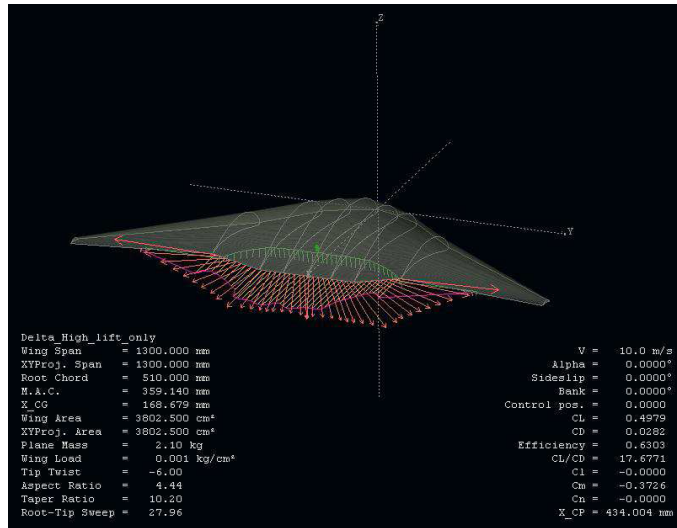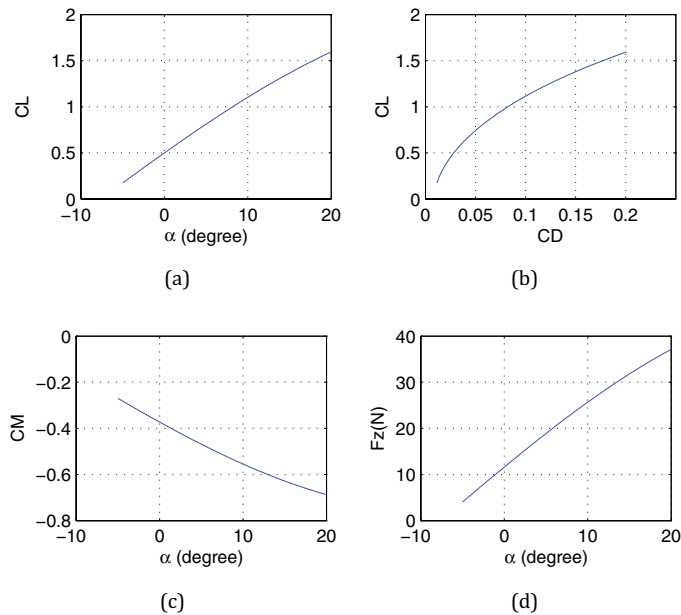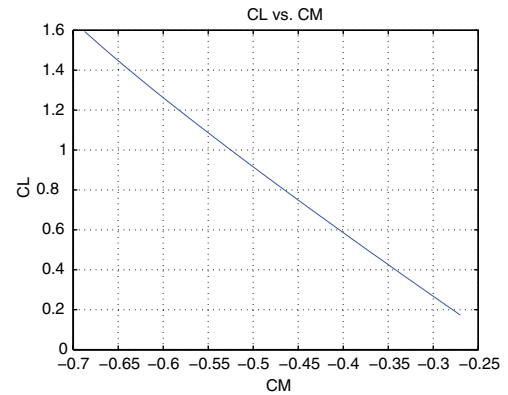From Fig. 18, a significant increase in lift coefficient can be viewed in the first chart. Even if the effective area for

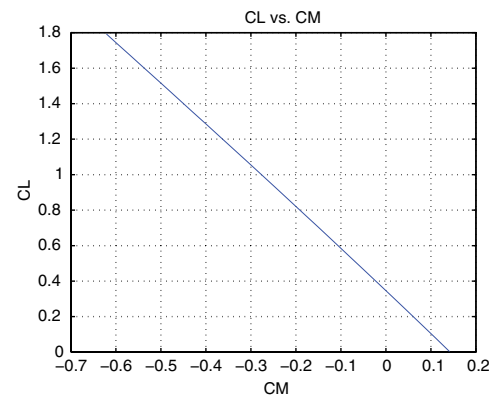Fig. 17.   XFLR5 simulation of the U-Lion Mark II.

Fig. 18.   Aerodynamic analysis of U-Lion Mark II with XFLR5. (a) CL versus AOAα, (b) CL versus CD, (c) CM versus AOAα and (d) lift versus AOAα.

(a)

(b)

Fig. 19.   Correlation between lift coefficient and pitching moment coefficient of U-Lion Mark II. (a) Without tail and (b) with tail.

aerodynamic forces is reduced to 3802.5 cm^2 from 5290 cm^2 for 1st prototype, the lift force reaches 20 N at the AOA of 5–6$°$, which verifies the effectiveness of the high lift airfoil. In terms of the pitching stability, according to Fig. 19(a), the system is still not a self-stable system or even worse than the first prototype, since at zero pitching moment, the lift coefficient is -0.25. Furthermore, in the real flight test of prototype Mark I, the effect of the control surfaces are not capable to balance the whole platform even at the highest control input according to the pilot experience. As a solution, an extra tail is added to balance the platform, as shown in Fig. 21. Two identical tails with one perpendicular to the plane surface and the other tilting downward 15$°$ are mounted to the main body to serve as elevator, rudder and landing skid. NACA 0012 airfoil is selected for the tail, the aerodynamic properties of which are shown in Fig. 20. Analysis of the platform with tail can be viewed in Fig. 22 and the fourth chart indicates that there is very little influence on the lift created even after the addition of the downward-tilting tail. In Fig. 19(b), the lift coefficient is also positive at the zero pitching moment. Thus,
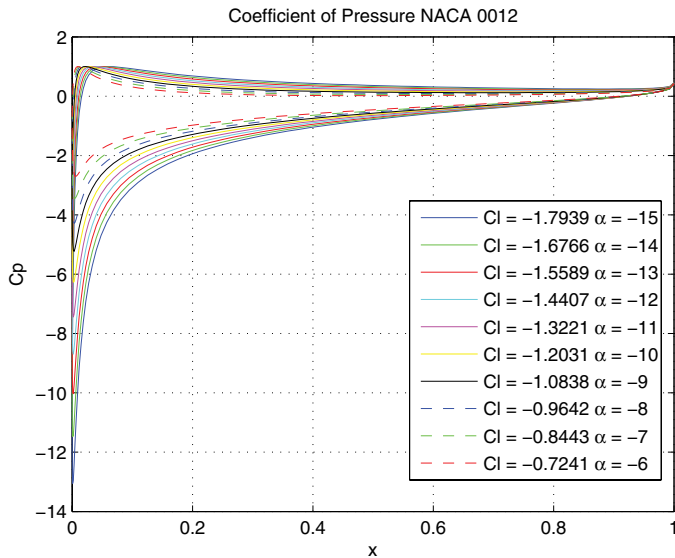
Fig. 20. Lift coefficient and pressure coefficient C_p distribution of airfoil NACA 0012.

this platform is a working prototype from simulation results.

One important point to note is that the aerodynamic efficiency of the simulated aircraft was very low as the swept wing design seems to work better at supersonic speeds and our operating velocity is far below that. This is explained in Sec. 5.1.

4.3. *Flight test*

With all the parts inclusive of the wings, fuselage and internal mechanisms completed in SolidWorks, the drawings
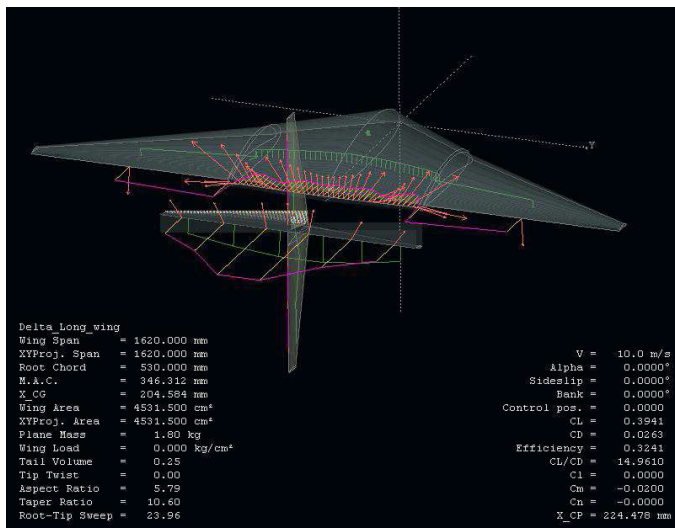

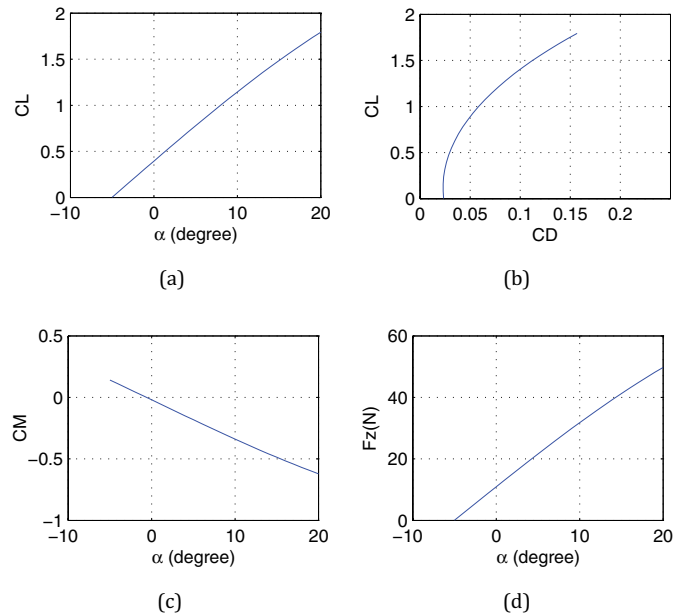Fig. 21. XFLR5 simulation of the U-Lion Mark II with tail.

Fig. 22. Aerodynamic analysis of U-Lion Mark II with tail. (a) CL versus AOAα, (b) CL versus CD, (c) CM versus AOAα and (d) lift versus AOAα.

Fig. 23. U-Lion Mark II (without tail).

were sent out for manufacturing. Wing and Fuselage are cut from 24 g/l EPP foam and the internal structures are made by carbon fiber sheets and aluminum. With the vectored thrust mounted on the top and a 3-cell battery inside, the whole platform weighs 2.3 kg, shown in Figs. 23 and 24. Even if this prototype perform better and cruise longer than the first prototype, it still ran out of control after several seconds. Further, in the VTOL mode, the vectored thrust is not powerful enough to lift the 2.3 kg platform and perform pitch, roll and yaw motions. Further weight reduction is indispensable to make a light and flyable platform.

Fig. 24.   U-Lion Mark II (without tail) with wings folded.

5.   Final Platform

After the two attempts at creating the hybrid platform using a delta-wing configuration, we instead decided to switch the wing profile from delta-wing to glider (see Figs. 25 and 26). There are several advantages in this change and they are depicted below.

5.1.   *Configuration change analysis*

There are two reasons that can account for the failures of delta-wing configuration:

(i) Crucial speed problem: The delta-wing configuration cannot provide enough lift force during flight transition when the flight speed is relatively low. This can be
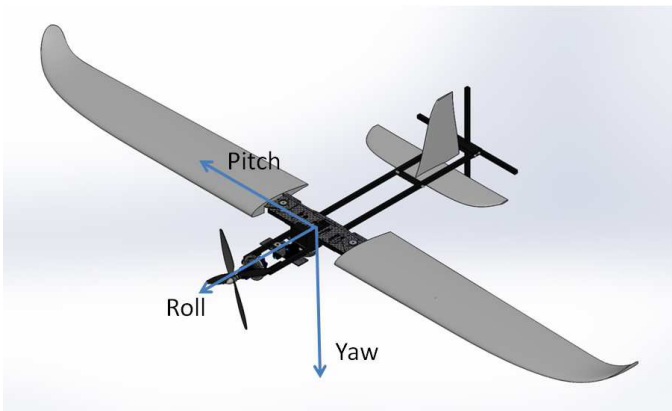

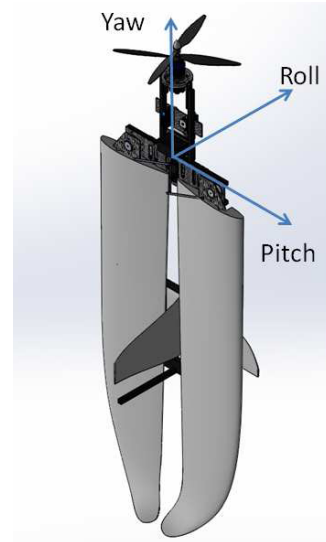Fig. 25.   U-Lion Mark III in Cruise mode.
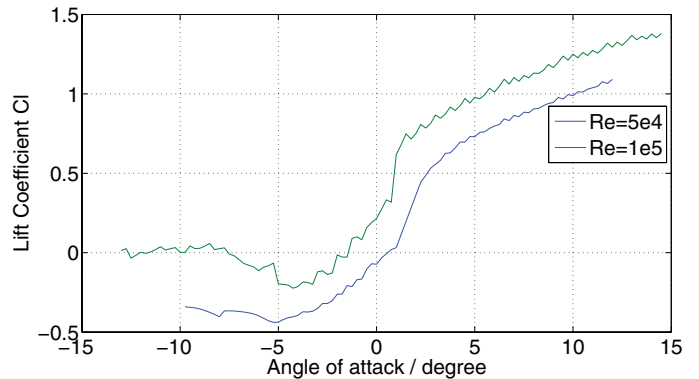

Fig. 26.   U-Lion Mark III in hovering mode.

Fig. 27.   Lift coefficient to AOA curve of airfoil CH10SM.

explained by the lift coefficient to AOA curve of airfoil CH10SM under different Reynolds numbers. As shown in Fig. 27, the upper curve is the curve for $Re = 1 \times 10^5$ while the lower one is for $Re = 5 \times 10^4$, thus great reduction in lift coefficient can be seen during $0°$ to $10°$ range.

(ii) Propeller vortex effect: From CFD results for delta-wing configuration, the lift force provided by the fuselage constitutes 36% of total lift force. However, the vortex effect from the propellers significantly affects the flow field on the fuselage surface. It can be predicted that the lift force generated from fuselage will be greatly reduced.

Thus, the glider-wing configuration is proposed as a viable solution because it can provide higher aspect ratio, and also the wing area affected by the propeller is much less than that from the delta-wing configuration.

5.2. *Aerodynamics analysis and computational fluid dynamics simulation*

The aerodynamics analysis is based on empirical methods for the airfoil [14, 16]. The wing parameters are shown in Table 1. To achieve high flight efficiency in Cruise flight, we adopt the notion from eagles with high aspect ratio wings. Clark Y airfoil is selected as our choice because of its advantage in low speed.

In the condition of 8 m/s flow velocity and $10°$ AOA, the Reynolds number is:

$$\text{Re} = \rho V l / \mu = 1.1 \times 10^5, \tag{8}$$

then the lift coefficient of Clark Y airfoil is estimated to be 1.3 using lift and drag coefficient curves generated by Profili software, which is shown in Fig. 28. Hence the lift force can be calculated as:

$$L = \frac{1}{2} C_l \rho V^2 S = 19.3 \, \text{N}. \tag{9}$$

Table 1. Wing parameters for fixed-wing configuration.

Parameter	Value
Reference wing area	$0.36 \, \text{m}^2$
Wing span	1.8 m
Wing chord length	0.2 m

Assisted by the vectoring thrust provided from the co-axial propeller and lift force from the fuselage, the lift force from the wings is sufficient to support the 2 kg weight of U-Lion in the Cruise flight.

5.3. *Vector thrust design*

Since U-Lion was designed to have VTOL, hovering and Cruise flight capabilities which requires the mechanism of thrust to be designed with the following features:

(1) For VTOL mode, the thrust is enough to lift the gross take-off weight of the aircraft.
(2) For full-envelope VTOL mode control, 3-axis attitude control should be realizable including pitching, rolling and yawing motions.
(3) For cruising mode, the mechanism is able to assist Cruise flight in fixed-wing mode.

The picture of the motor is shown as Fig. 29. As estimated, the overall take-off weight is around 2 kg inclusive of the battery. Thus, the co-axial contra-rotating rotor is able to provide at least 3.5 kg thrust for the purpose of attitude control and maneuverability. After a survey for the commercial off-the-shelf brushless motors, a brushless motor with 1100 Kv value is selected to build the contra-rotating rotor. It is shown in Fig. 29 that the shaft in the upper motor was removed and an extended lower motor shaft is used in its stead. A bearing is inserted between the upper motor and the lower motor shaft to realize the free movement
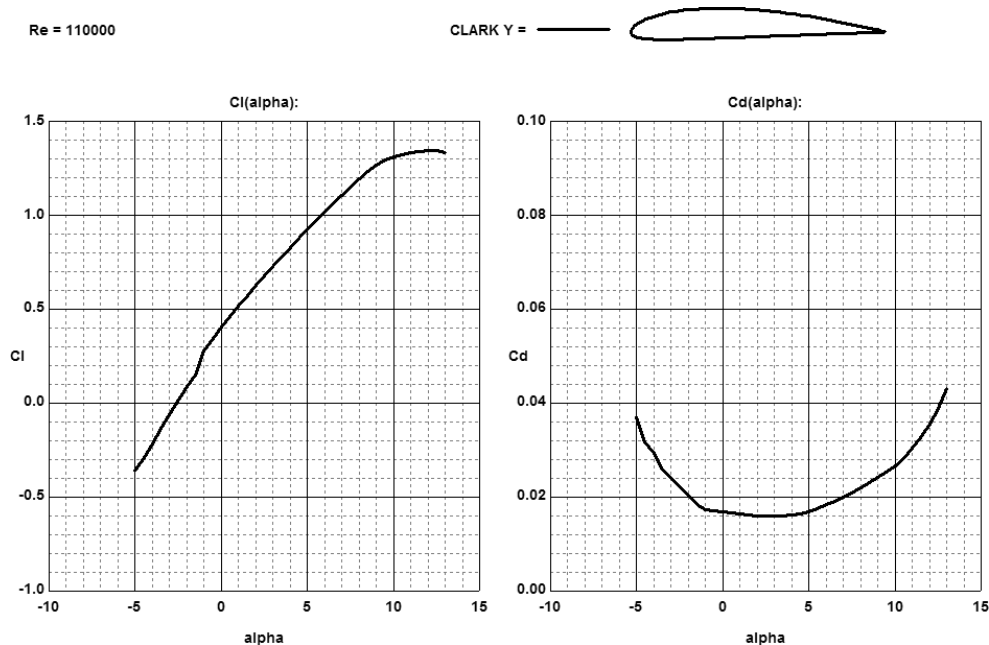

Fig. 28. Lift and drag coefficient curves of Clark Y airfoil when $\text{Re} = 1.1 \times 10^5$.

Fig. 29.   The self-customized contra-rotating motor.

between the two rotors. A 11×7 pusher propeller is fixed onto the shaft and a smaller counterclockwise 10×5.5 propeller is screwed on the upper motor. In the hovering condition, the torque of each rotor is counterbalanced with the same RPM and yawing motion is created with the difference between the upper and lower rotor.

As shown in Fig. 30, for pitching and rolling motions, a gimbal device is installed to realize the vector thrust pointing to any desired direction. An aluminum inner ring is fastened with the outer ring by two bearings between them and the outer ring is assembled on the top of the aircraft. Both of the gimbal rings are attached with a linkage supported by a servo. The angle of the servo horn could be controlled to realize a certain angle of the gimbal ring which results in a full-envelope control of the UAV. With this vector-thrust contra-rotating motor, *x*-axis and *y*-axis rotating motions are realized. To create a greater yaw motion,
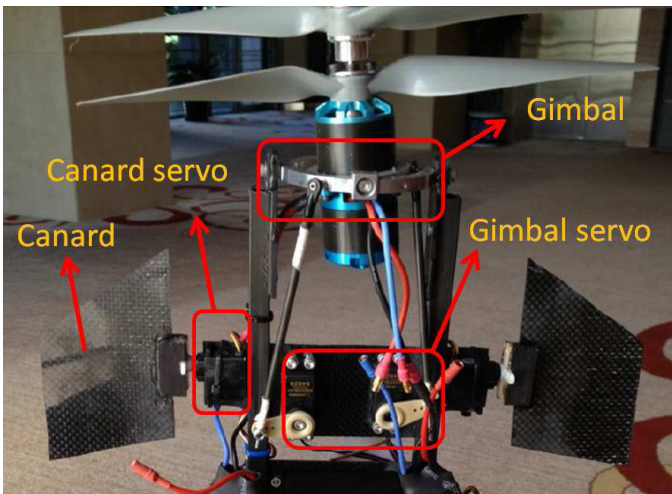
two rotating canard wings are designed in the down flow areas of propellers to assist yaw control in the VTOL mode.

5.4.   *Reconfigurable wing design*

The tail-sitter is capable of two flight modes: Cruise flight mode and VTOL mode. For Cruise flight mode, a larger wing span is preferable to generate more lift at a lower speed. For VTOL mode, the aircraft has to maintain a small footprint to reduce the effect of wind disturbance. The fully extended wing in the VTOL mode also makes it harder for the vehicle to maneuver in the heading direction. Keeping this tradeoff in mind, we came out with a reconfigurable wing design which extends the wing in cruising mode and retracts the wing in VTOL mode. To keep the system structure simple and minimize the platform weight, the reconfiguration is implemented using a four bar linkage design [15]. The design procedure and implementation details will be covered in this section.

5.4.1.   *Four-bar linkage design*

The design of four-bar system involves the determination of four bars' length subject to a set of constraints. In this design, we have the following constraints:

(1) Single servo driving: To simplify the system structure and reduce the weight of the system, we design two sets of four-bar linkage system which use only one driving servo. As shown in Fig. 31, there are two sets of four bar linkage mechanisms, $\{OABE\}$ and $\{OCDF\}$. The three revolute joints (O, E, F) are fixed to the air frame. Joint B and D are attached to the two sets of wings. While the servo drives the bar CA to sweep a certain angle around joint O, both EB and FD will change accordingly, adjusting the wings' spanning angle.
(2) Minimum load on servo: In order to exert minimum load on the servo bar OA, especially when the wings are fully extended, one extreme position is set to the position where the rocker OA and the coupler AB are

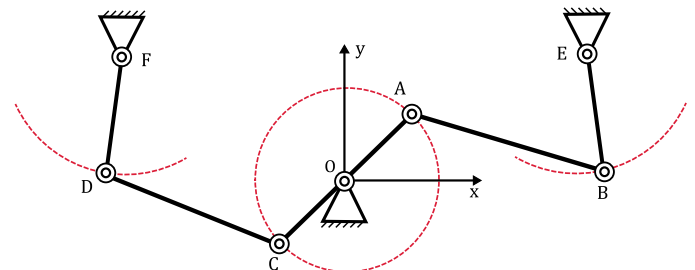

Fig. 30.   The propulsion system.
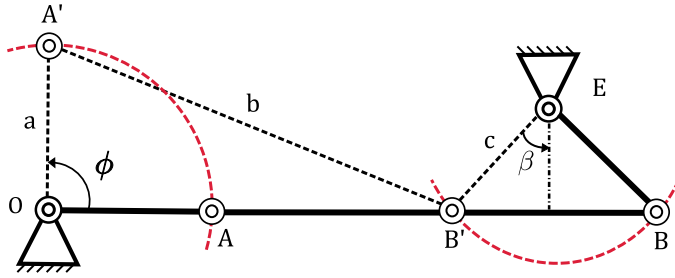

Fig. 31.   Symmetric four-bar linkage system.

Fig. 32. Parameter determination of four-bar linkage.

co-linear with each other (Fig. 32). In this condition, the load induced by the right wing are compensated by the one from the left wing. This corresponds to the case when the wings are fully extended. In the other aspect, in order to effectively extend the wings from vertical mode to horizontal mode, the transmission angle between *AB* and *EB* cannot be too small or large. We design the transmission angle to be in the range of $[45°, 90°]$.

(3) Wing sweeping angle: To fully extend and retract the wings between horizontal mode and vertical mode, the sweep angle of the wing are designed to be $90°$, denoted by 2β in Fig. 32. What is more, the sweeping angle of the rocker *OA* is defined as ϕ and set to be $90°$. The two extreme positions of the reconfigurable wing are labeled as *OABE* and *OA'B'E* in Fig. 32.

In practice, referring to Fig. 31, the distance between revolute joints *E* and *F* is determined by the overall vehicle frame size. The length rocker arm *OA* and *OC* is defined by the available servo horn length. With all the above constraints, we could derive the length of linkage bar system as

$$EB = \frac{0.5\,EF \cdot OA}{(EF - OA)\sin\beta}, \qquad (10)$$

$$AB = 0.5\,EF - OA + EB\sin\beta. \qquad (11)$$

With the specified constraints and Eqs. (10) and (11), we could derive the parameters of four bar linkage system as shown in Table 2.

Table 2. Parameters of four bar linkage.

Parameter	Value
OA/OC	38 mm
AB/CD	109.4 mm
EB/FD	31.68 mm
EF	250 mm
Rocker sweeping angle	90°

5.4.2. *Four-bar linkage implementation*

With the designed four-bar linkage parameters determined, we build the reconfigurable wing structure as shown in Figs. 33–35. Figure 34 illustrates the case when the wings are fully extended for Cruise flight and Fig. 35 demonstrates the retracted wing configuration for VTOL mode.

5.5. *Bearing holder design*

The wing-body joint consists of two bearings mounted at wing root by a bearing holder, and a shaft mounted on the body. During Cruise flight, lift forces on the wings result in a
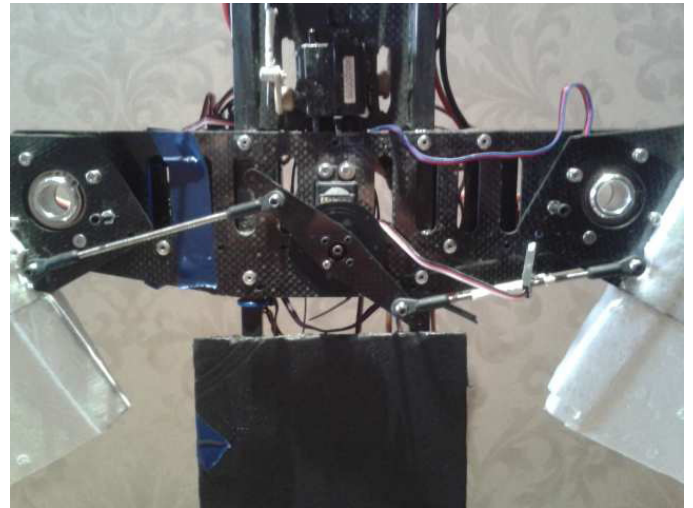

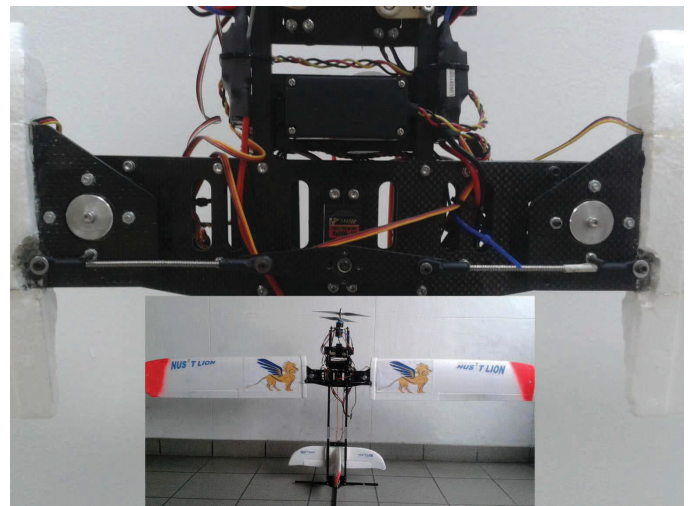Fig. 33. Driving mechanism for reconfigurable wing.

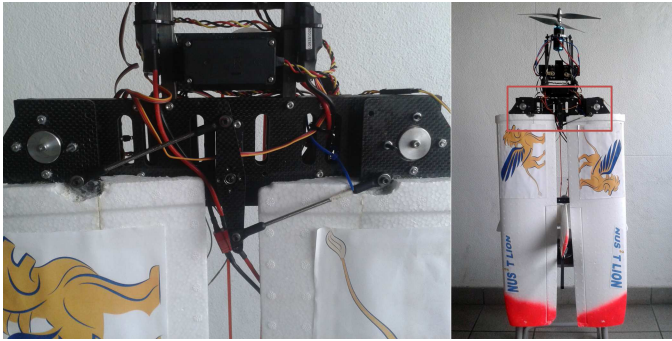Fig. 34. Extended wing configuration.

Fig. 35.   Retracted wing configuration.

Fig. 37.   Cross section of wing-to-body joint.

thrust force and a torque at wing-body joints. A typical ball bearing is designed to withstand a large amount of radial load and a moderate amount of axial load, but it is not designed to take torsional loads [17]. In contrast, the two-bearing configuration can provide a torque as a couple of two radial forces, thus ensures that the joint is strong enough under both thrust and torsional loads (see Figs. 36 and 37).

5.6.   *Adaptive CG*

The CG of an aircraft should be located around the center of lift of the wings during Cruise. On the other hand, during VTOL and hovering, the CG should be located as far away from the propellers as possible, based on our experiences from flight tests. The adaptive CG mechanism is able to reposition the CG of the aircraft to a certain extent, so that the CG requirements for both Cruise and VTOL/hovering could be met [11].

CG position is adjusted by moving the heaviest component on the aircraft, i.e., the battery. It weighs 300 g, about one seventh of the total mass of the aircraft. During Cruise flight, the battery is located immediately after the central plates. The separation between the central plates and the
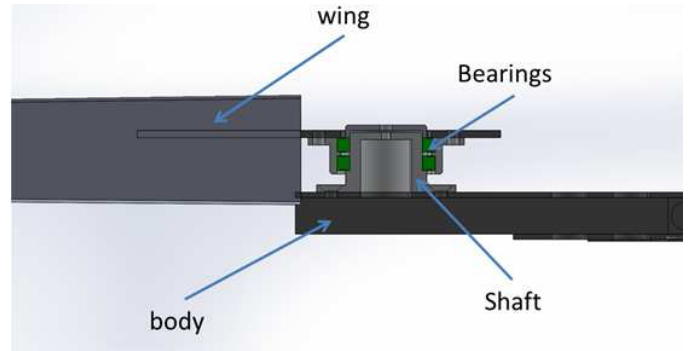
tail, i.e., the maximum distance that the battery can travel, is 40 cm. By pushing the battery all the way from the center to the tail, the CG of the aircraft can be pushed towards the tail by 5 cm. The mechanism to move the battery consists of a pulley near the tail, a servo motor near the propeller, a belt and a slider on the fuselage as seen in Fig. 38. The battery is strapped to the slider which is attached to the belt. The servo turns the belt, and the battery moves accordingly.

Although it is not the definitive solution to the CG problem between transitions, the adaptive CG mechanism has proved to be helpful. During our flight tests, significant improvement in hovering stability is observed after installing the mechanism. However, stability in VTOL/hovering modes turns out to be affected by more than CG position alone. Large surface area, inadequate power from propeller and other unknown factors could all have contributed to the instability, which is why adaptive CG mechanism alone cannot completely solve the stability problem.

In conclusion, the current version of adaptive CG mechanism is a promising solution to the stability problem between transitions. Further improvement in the mechanism, as well as a more thorough understanding of the
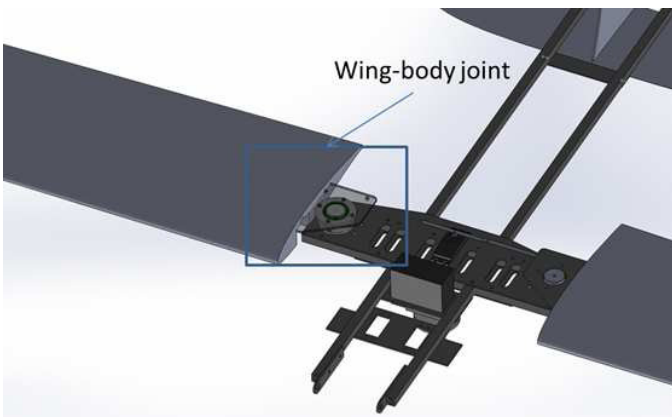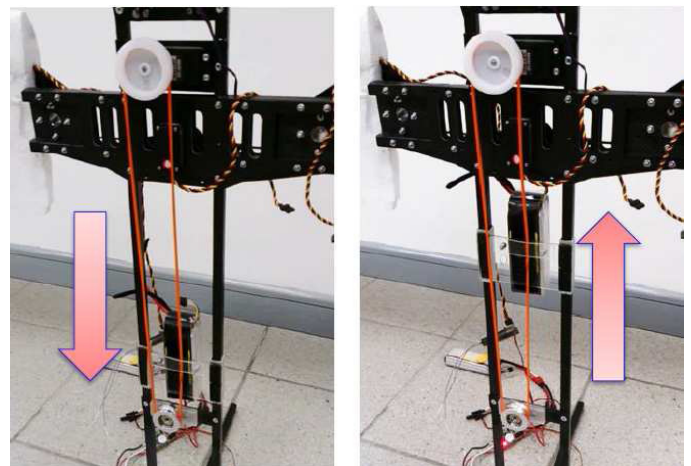

Fig. 36.   Wing-to-body joint.

Fig. 38.   Adaptive CG mechanism.

causes of instability, are necessary to completely address the stability issue.

5.7. *Electronic configuration*

The electrical components are listed in Table 3. The motor is a self-customized contra-rotating motor, the maximum lifting force generated is around 35 N, which is able to support the hovering and maneuverability in VTOL mode. The two electrical speed controller (ESC) are chosen to be DualSky 40XC4018BA for the accuracy of controlling the speed of the motors. The weight of the ESC is 30 g and the maximum current allowed is 40 A which is suitable for the control of the rotating motor.

In this U-Lion design, there are quite a few actuators with different requirements. Based on the requirements, different servos are chosen for minimum weight and larger safety margin. The specifications of the selected servos are listed in Table 4. The servo used for supporting the gimbal mechanism is selected to be the Airtronics 94141Z. The gimbal support servo must have a fast response for good controllability and the torque has been large enough for supporting the gimbal movement. Since the maximum tilting angle of the gimbal is $30°$ and the radius of the gimbal is

Table 3. List of electrical components.

Component	Part number
Motor	Himax CR3516
Propellers	APC 11×5.5P & 10×7
ESC	Dualsky 40 XC4018BA
Gimble servo	Airtronics 94820 Servo
Four bar mechanism servo	HS7950TH
Wing control surface servo	HS-65MG
Tail control surface servo	HS-85MG
Canard servo	HS-65MG
Gyro	Futaba GY240
Receiver	Futaba R6014HS
Transmitter	Futaba 14FG
Battery	4S 2200 mAh

Table 4. Specifications of servos.

Component	Part no.	Torque (kg cm)	Speed (s/60°)	Weight (g)
Gimble servo	Airtronics 94820	4	0.16	32.9
Four bar servo	HS7950TH	29	0.15	68
Wing control servo	HS-65MG	2	0.11	10
Tail control servo	HS-85MG	3.5	0.14	21.83
Canard servo	HS-65MG	2	0.11	10

3 cm the maximum torque generated to the gimbal is approximately $2 \times \sin 30° \times 3 = 3$ kg cm. The selected Airtronics servo fulfils the requirement with maximum torque of 4 kg cm with a response speed of 0.16 s/60°. The weight of the Airtronics servo is 32.9 g which is light for U-Lion.

The wing control surface servos and canard servos are selected to be HS-65MG servo. The main reason to select this servo is because of its light weight. The HS-65MG servo only weighs 10 g while providing a relatively high torque of 1.5 kg cm and a fast response speed of 0.11 s/60°. For the tail control surface servo, since the tail control surface requires larger torque and more stable response, the servo is selected to be HS-85MG. The HS-85MG servo has a higher torque of 3.5 kg cm and the weight is 21.83 g.

The servo for the four bar mechanism is selected to be HS7950TH which has a high torque and low weight. Based on the four bar mechanism calculation and the weight of the wings, in order to support the foldable wings, the servo has to provide a torque of at least 15 kg cm. The HS7950 servo could provide a torque of 29 kg cm which fulfils the requirement with a safety factor of around 2. The weight of the servo is 68 g which is lower than other servos that have similar torque. The reaction time for the servo is 0.15 s/60° which provides a prompt response for the wing folding. The main controller for the VTOL mode is the gyro controller, which serves as a proportional controller for the attitude control. The gyro is selected to be Futaba GY240. The gyro has a very accurate gyro sensor and fast controlling rate (70 Hz) which is suitable for U-Lion.

5.8. *Material stress analysis*

Based on flight tests, the most vulnerable part of the fuselage is determined to be the central plate. A preliminary structural analysis of the central plate is thus conducted.

As shown in Fig. 39, the reactions at the wing-body joint consist of one force and one moment. Assume that sections of the plate glued to carbon fiber square tubes are fixed (Fig. 40), and that load is applied to the plate at where the bearing holder and the plate contact (Fig. 41). The load on the plate is equivalent to 10 N of lift at the center of each wing ($mg/2 = 10$ N in Fig. 39) with a safety factor of 1.5.
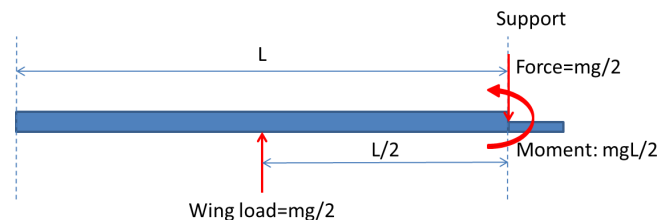

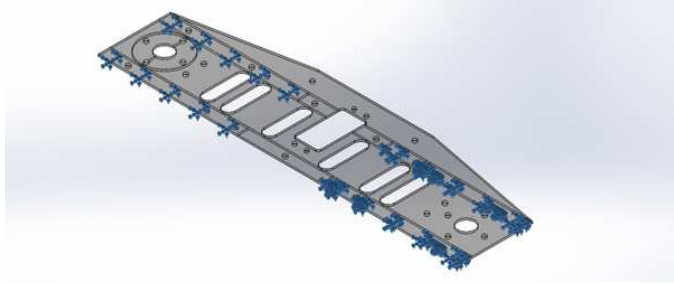Fig. 39. Free body diagram of a wing.
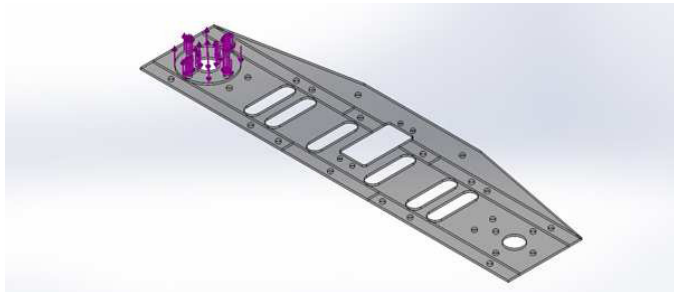
Fig. 40.   Fixtures in FEM simulation.

Fig. 41.   Load in FEM simulation.

With this setup, a finite element method (FEM) simulation is carried out using SolidWorks Simulation. As shown in the figure, the maximum stress (Fig. 42) is well below the yield strength of carbon fiber, and the displacements are negligible (Fig. 43).
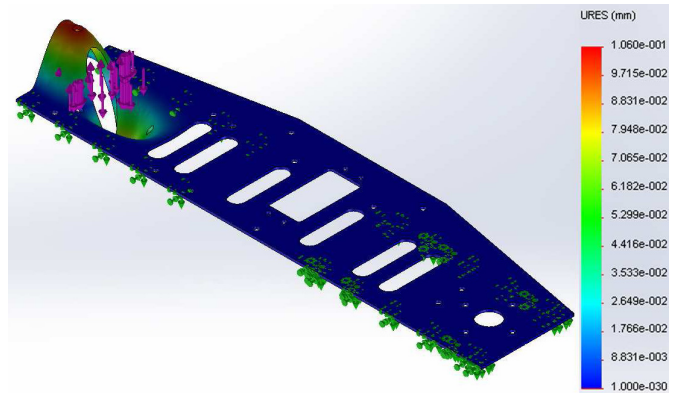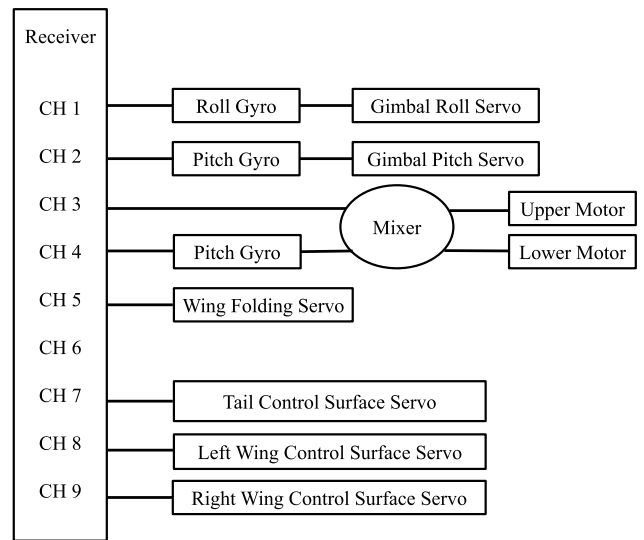
5.9.   *Control modes*

The control methods for VTOL mode and Cruise flight mode are quite different for a UAV. For conventional VTOL UAV, such as helicopter or coaxial helicopters, the VTOL six degree control is achieved by varying the angle of the rotor plane. However, for the fixed wing plane, the motion control
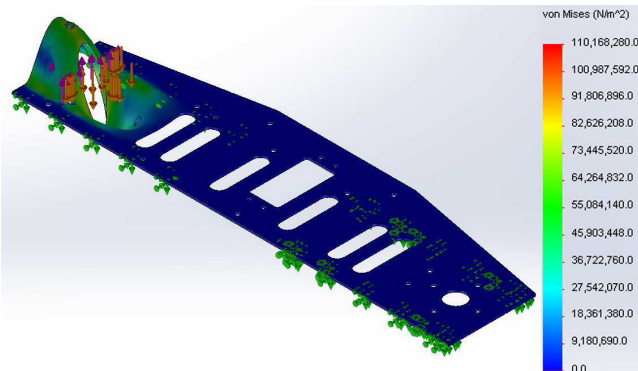

Fig. 42.   Stress simulation.

Fig. 43.   Displacement simulation.

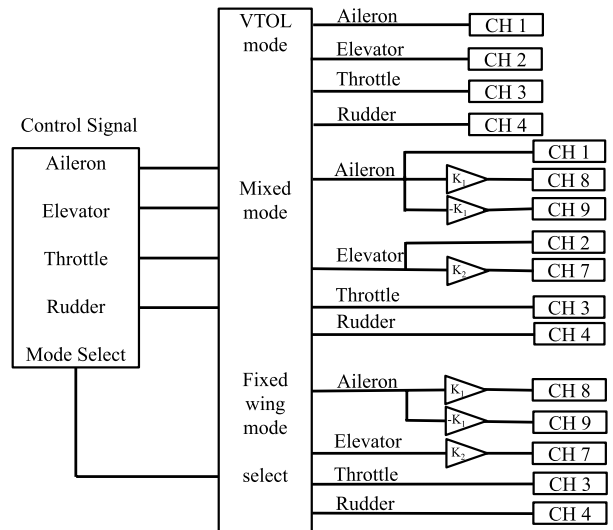Fig. 44.   The control circuit of U-Lion.

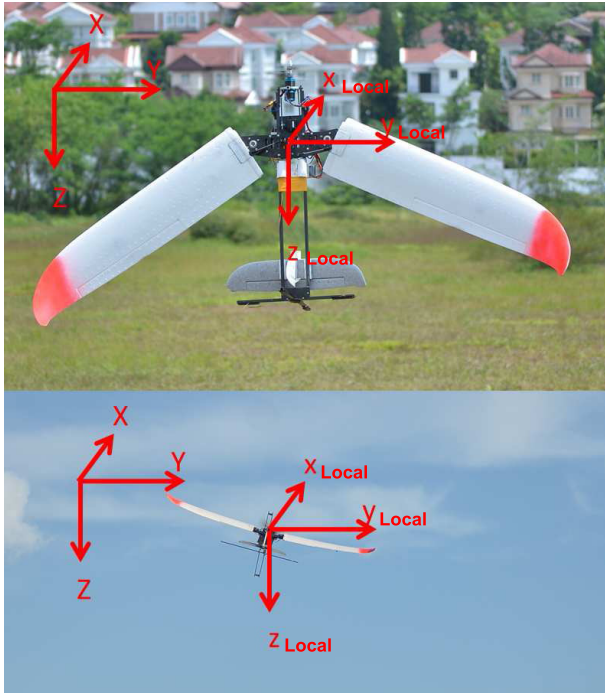Fig. 45.   The control logic of U-Lion.

Fig. 46. The coordinate definition of U-Lion.

is achieved by the control surface on the wings or the tails. The difficulty of unconventional UAV with VTOL and Cruise flight ability lies greatly in how to combine the two control modes as well as the transition between the two modes. In our UAV design, we adopt the vector trust for VTOL control and control surface for the Cruise flight control.

The control involves three modes of control, i.e., VTOL mode, fixed wing mode and the mixed control mode. The U-Lion is controlled manually at the current stage. The onboard electronic circuit mainly consists of a receiver and extending components, as shown in Fig. 44. The control logic is programmed in the transmitter as shown in Fig. 45. Defining the global coordinate as the standard North–East–Down (NED) *XYZ* frame with *X*-axis pointing north, *Y*-axis pointing east and *Z*-axis pointing down. VTOL flight requires the motor to be pointing in the negative *Z*-direction and Cruise flight requires the motor pointing in *XY* plane. Defining the local frame of U-Lion to be $x_{local}y_{local}z_{local}$ with z_{local}-axis pointing down, y_{local}-axis pointing to the right wing and parallel to the *XY* plane, x_{local}-axis perpendicular to the *y*-axis and *z*-axis following the right hand rule. The coordinates are shown in Fig. 46. Due to the special tail sitter design, we can see that the pitch, roll and yaw movement

Fig. 47. The flight of U-Lion on the competition day.

Table 5.   U-Lion Mark III specifications.

Weight	2.2 kg
Max thrust	40 N
Max cruise speed	10 m/s
Flight endurance	10 min
Dimensions	2.2 m × 0.9 m × 0.3 m

agrees in both VTOL mode and Cruise mode. Thus it allows a smooth transition in control signals between VTOL and Cruise mode. This results in a clear control logic for manual control and paves the way for future automated control.

The transition between VTOL mode and Cruise mode requires the U-Lion to transform from vertical flight into horizontal flight. The mixed control mode serves as an important bridge between VTOL mode and Cruise mode. The change of pitch angle of the vector trust will push the head down and the elevator on the tail also assists this transition process. The control surface on the wings will help to stabilize the UAV during transition. After transition, the wing and tail control surfaces can effectively control the UAV and the control mode is switched to Cruise mode.

5.10.   *Test results*

The flight on the competition day at Beijing is shown in Fig. 47. The specifications of U-Lion can be found in Table 5. The subfigures in the figure is cropped from the video taken on the day with 0.25 s time difference each. From the figures we can see a very smooth transition between the VTOL mode and the Cruise flight mode. The flight shows a very good dynamics performance of the U-Lion. Our YouTube video could also be found in the following link: http://www.youtube.com/watch?v=3IUzbc_N5K4.

6.   **Conclusion**

In this paper, we presented the development and implementation of the U-Lion that has been solely designed by the National University of Singapore Unmanned System Research Group. U-Lion has been designed with a reconfigurable wing and a tail-sitter structure, which combines the advantages of a fixed-wing plane and a rotor helicopter effectively. During the competition, U-Lion has demonstrated that it could transit from vertical takeoff to a hovering stage before flying in Cruise mode to realize efficient long duration flight. U-Lion also performed well in the creative category with the special internal designs that empowered its capabilities. These are namely, the reconfigurable wings, the adaptive CG and the unique contra-rotating thrust-vectored propulsion system.

Further experiments are in progress to obtain a reliable and accurate dynamic model of the U-Lion such that we can fulfill fully-autonomous flight in the future. In addition, we intend to implement intelligent algorithms such as vision-based techniques in obstacle avoidance and target tracking to allow the U-Lion to be used in multi-task autonomous missions.

References

[1]   K. Z. Ang, J. Cui, T. Pang, K. Li, K. Wang, Y. Ke and B. M. Chen, Development of an unmanned tail-sitter with reconfigurable wings: U-Lion, *11th IEEE Int. Conf. Control & Automation (ICCA)* (IEEE, 2014), pp. 750–755.

[2]   J. A. Guerrero, R. Lozano, G. Romero, D. Lara-Alabazares and K. C. Wong, Robust control design based on sliding mode control for hover flight of a mini tail-sitter unmanned aerial vehicle, *35th Annual Conf. IEEE Industrial Electronics, 2009. IECON'09* (IEEE, 2009), pp. 2342–2347.

[3]   K. Jackson, J. Li, E. Timmons and J. Wallace, icarusLabs: An adventure in crowdsourcing, *Unmanned Syst.* **1**(2) (2013) 199–209.

[4]   E. Cetinsoy, E. Sirimoglu, K. T. Oner, C. Hancer, M. Unel, M. F. Aksit and K. Gulez, Design and development of a tilt-wing UAV, *Turk. J. Electr. Eng. Comput. Sci.* **19**(5) (2011) 733–741.

[5]   H. Stone, Aerodynamic modelling of a wing-in-slipstream tail-sitter UAV, *2002 Biennial International Powered Lift Conf. Exhibit*, Williamsburg (2002), pp. 5–7.

[6]   J. Escareno, R. H. Stone, A. Sanchez and R. Lozano, Modeling and control strategy for the transition of a convertible tail-sitter UAV, *European Control Conf.* (2007), pp. 2–5.

[7]   W. Shyy, H. Aono, S. K. Chimakurthi, P. Trizila, C. K. Kang, C. E. Cesnik and H. Liu, Recent progress in flapping wing aerodynamics and aeroelasticity, *Prog. Aerosp. Sci.* **46**(7) (2010) 284–327.

[8]   www.rheinmetall.com.

[9]   G. Cai, L. Feng, B. M. Chen and T. H. Lee, Systematic design methodology and construction of UAV helicopters, *Mechatronics* **18**(10) (2008) 545–558.

[10]   M. Drela, XFOIL: An analysis and design system for low Reynolds number airfoils, in *Low Reynolds Number Aerodynamics* (Springer Berlin Heidelberg, 1989), pp. 1–12.

[11]   I. Palunko and R. Fierro, Adaptive control of a quadrotor with dynamic changes in the center of gravity, in *Proc. 18th IFAC World Congress*, Vol. 18 (2011), pp. 2626–2631.

[12]   J. J. Bertin and M. L. Smith, *Aerodynamics for Engineers*, Vol. 1 (Englewood Cliffs: Prentice Hall, 1989).

[13]   J. D. Anderson Jr., *Fundamentals of Aerodynamics* (Tata McGraw-Hill Education, 1985).

[14]   E. N. Jacobs, K. E. Ward and R. M. Pinkerton, The characteristics of 78 related airfoil sections from tests in the variable-density wind tunnel, Report No. NACA-TR-460, National Aeronautics and Space Admin Langley Research Center Hampton, VA (1933).

[15]   R. R. Bulatovic and S. R. Dordevic, Optimal synthesis of a four-bar linkage by method of controlled deviation, *Theor. Appl. Mech.* **31**(3–4) (2004) 265–280.

[16]   H. R. Kelly, The estimation of normal-force, drag, and pitching-moment coefficients for blunt-based bodies of revolution at large angles of attack, *J. Aeronaut. Sci.* **21**(8) (2012).

[17]   J. E. Shigley, *Shigley's Mechanical Engineering Design* (Tata McGraw-Hill Education, 2011).

[18]   P. Kurowski, *Engineering Analysis with SolidWorks Simulation 2013* (SDC Publications, 2013).